Characterization of a Regenerable Impactor Filter for Spacecraft Cabin Applications

Juan H. Agui[1]
NASA Glenn Research Center, Cleveland, OH 44135

R. Vijayakumar[2]
Aerfil, Liverpool, NY 13088

Regenerable filters will play an important role in human exploration beyond low-Earth orbit. Life Support Systems aboard crewed spacecrafts will have to operate reliably and with little maintenance over periods of more than a year, even multiple years. Air filters are a key component of spacecraft life support systems, but they often require frequent routine maintenance. Bacterial filters aboard the International Space Station require almost weekly cleaning of the pre-filter screen to remove large lint debris captured in the microgravity environment. The source of the airborne matter which is collected on the filter screen is typically from clothing fibers, biological matter (hair, skin, nails, etc.) and material wear. Clearly a need for low maintenance filters requiring little to no crew intervention will be vital to the success of the mission. An impactor filter is being developed and tested to address this need. This filter captures large particle matter through inertial separation and impaction methods on collection surfaces, which can be automatically cleaned after they become heavily loaded. The impactor filter can serve as a pre-filter to augment the life of higher efficiency filters that capture fine and ultrafine particles. A prototype of the filter is being tested at the Particulate Filtration Laboratory at NASA Glenn Research Center to determine performance characteristics, including particle cut size and overall efficiency. Model results are presented for the flow characteristics near the orifice plate through which the particle-laden flow is accelerated as well as around the collection bands.

Nomenclature

d	=	particle diameter
C_c	=	Cunningham Correction Factor
Re	=	Reynolds number
U	=	jet velocity
St	=	Stokes number
W	=	jet width
λ	=	molecular free mean path
ε	=	collection efficiency
ρ_p	=	particle density
η	=	viscosity

[1] Aerospace Engineer, Fluid Physics and Transport Branch, and 21000 Brookpark Rd, Mail Stop 77-5, Cleveland OH 44135.
[2] President, Liverpool, NY 13088

I. Introduction

HUMAN exploration beyond low Earth orbit (LEO) will require spacecraft systems with ever increasing reliability and operational longevity. The cost of launch mass and the logistics of resupply impose very tight and challenging constraints on the structural and operational design of space-bound hardware. In this case, systems that save on mass, volume, and power, and that last the length of the mission with minimal maintenance are attractive alternatives over current state of the art (SOA) systems.

The particulate filtration system is a crucial component of the air revitalization system. The practice for commercial filters is to replace the filter element on a routine schedule to prevent clogging or excessive pressure drops. For example, the ISS uses a HEPA filter cartridge with a Nomex screen pre-filter to capture most of the airborne particles and fibrous matter generated in the cabin volume. Particulate load models that take into account the different sources of generation have been developed for the Space Station[1], which show a significant source of fibrous matter in the range from 10 to 50 μm that the Nomex screens tends to capture. These filters are replaced periodically depending on location on the ISS and loading conditions. While the HEPA element is replaced periodically on a 2.5 to 5 year cycle[2], the face of the Nomex screen is maintained on an almost weekly basis, mostly through vacuum cleaning, which significantly taxes valuable resources (power, crew time, waste disposal).

In general, high efficiency media and devices are optimized for capturing very small particles, but they can become prematurely loaded if exposed to a moderate concentration of large particles over long periods. Therefore, one or more stages of pre-filtration can be effective in capturing large size matter before it affects the high efficiency filter. Also, pre-filter stages generally do not require high efficiency media and therefore they may be more amenable to regeneration or cleaning. A Scroll Filter system is being developed at the NASA Glenn Research Center to address the needs for long duration missions. The filter system consists of two stages: the scroll media and an impactor filters. The performance of the Scroll Filter system in parabolic flights has been previously reported [see Ref. 3], which indicated that further studies were needed under more controlled conditions than the short periods of microgravity would allow.

This paper reports on new performance data on the Impactor filter using improved testing techniques.

II. The Scroll Filter

The Scroll Filter provides regeneration capability, autonomy, and several-fold increases in operational longevity over SOA filter systems. It is a multi-stage filtration system consisting of a regenerable impactor filter stage and a scroll media (self-replacing media) filter stage. An optional high efficiency media stage can be added if tight requirements on fine and ultrafine particulates are warranted. Figure 1 shows the filter media in the scroll stage and different views of the impactor filter stage. Figure 1b shows a close up of the orifice plate where the flow converges and is accelerated, and Fig. 2b shows the backside showing the bands (endless belts) that collect the particles. More details of the different components and other hardware details may be found in Ref. 3.

Although the impactor stage was designed with impactor principles in mind, several simplifications were made in order to reduce mass and complexity. For one, instead of having a contoured nozzle to produce the jet, a simple flat plate with an array of eight slits was used. The slits help to distribute the flow through several parallel stages of impactors. In another modification, the impactor stage uses an endless belt (or flexible band) instead of a single impaction plate in order to provide a means of regeneration. The first surface, as seen in Fig. 2, serves as the impaction surface. A small layer of compatible (low toxicity and offgassing) grease is applied to the impaction surface to increase particle adhesion. When the surface is covered extensively with particles, or if a thick layer of particles has grown to a thickness that makes adhesion ineffective, the surface needs to be regenerated. At this point, the band is rotated so that the loaded surface passes by a scrapper that removes the layer of particles in the form of a paste because of the grease sublayer. At the same time a clean segment of the band revolves around to the front and becomes exposed to the jet flow, in effect regenerating the impactor stage.

Data on the performance of the Scroll Filter system in parabolic low-g flights has been previously reported. Although the microgravity environment provides a relevant environment for space applications and removes the settling aspect of challenge aerosols, it is constraining in that testing has to be performed in repeated short time segments of about 20 seconds. Before transitioning to low-g conditions the aircraft goes through a high-g period that can produce remnant transients, particularly as the challenge aerosols are released into the flow. Additionally there are size constraints imposed, due to safety concerns, which limit the size of hardware that can be flown.

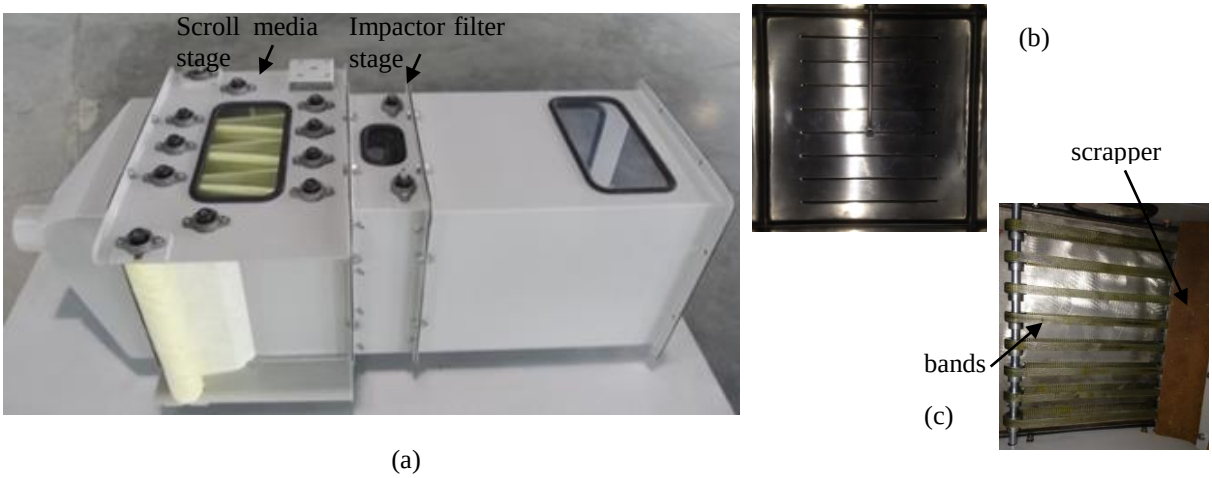

Figure 1: Pictures of Scroll Filter system. (a) filter assembly, (b) orifice plate, (c) impaction bands with scrapper.

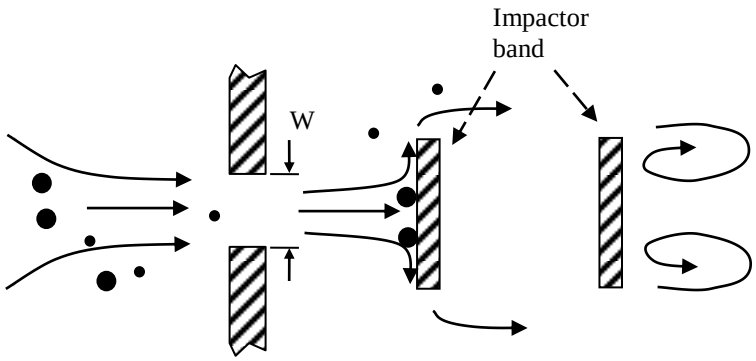

Figure 2: Depiction of impactor flow.

III. Particle Collection Technique

The principle of inertial impaction is well established. Particles are captured by virtue of their inertia which, if sufficiently massive, causes them to separate from curved flow streams. Since the size of the particle correlates with its inertial mass, for homogeneous properties, the capturing mechanism at a given jet velocity is size dependent. The graphic in Fig. 2 depicts the fate of different size particles as they pass through the impactor. The high turning angle encountered near the bluff impaction surface, causes relatively large particles to impact onto the surface while the smaller particles, which are well entrained in the flow, circumvent the impaction surface and continue downstream with the flow.

Aerosol transport near walls and around obstructions is characterized by the particle's Stokes number. In the case of an impactor surface the Stokes number is given by[4]:

$$St = \frac{\rho_p d_p^2 C_c U}{9\eta W} \tag{1}$$

Where ρ_p *and* d_p are particle density and diameter, W is the jet width, C_c is the Cunningham Correction Factor, η is the gas viscosity, and U is the jet velocity.

For an impactor, the collection efficiency curve is quite steep and is represented by the d_{50}, i.e. the particle diameter for which particles are collected with 50% efficiency, and an associated critical Stokes number, St_{50}. The critical Stokes number is a key parameter in the design of the impactor and its value is uniquely prescribed for the type of orifice. Typically a value of 0.59 for the critical Stokes number is prescribed for a rectangular orifice opening (and 0.24 for round jet).[4] The d_{50}, also known as the impactor cut size, is determined from the critical Stokes number and can be found from equation 2.

$$d_{50} = \sqrt{\frac{9W^2 St_{50}}{C_c \rho_p \,\mathrm{Re}}} \tag{2}$$

Here the Reynolds number is based on the jet width, W. An initial value of d_{50} can be obtained from Eq. 2 by first assuming a Cunningham Correction Factor value of 1. After this, the following relation can be used in iterative process to determine the numerically converged value.

$$C_c = 1 + \frac{\lambda}{d_p}\left[2.514 + 0.8e^{\frac{-0.55 d_p}{\lambda}}\right] \tag{3}$$

Here λ is the molecular mean free path of the gas having the same units as the particle diameter, d_p.

IV. Modeling

The wake flow behind an impactor surface can be quite complex, typically dominated by shedding vortices. This has implications for particle measurements conducted downstream of an impactor. In the present case, the unconventional impactor geometry, which includes two impactor bodies (front and back of the impaction band as seen in Fig. 2) and multiple adjacent impactor stages, generates additional flow complexities. The significance is that the hydrodynamic forces on the particles are strongly affected by flow behavior which in turn influences particle concentration and size measurements. Modeling of the jet flow through the impactor orifice and wake flow field helped to provide some insight in interpreting the particle measurements obtained in testing.

Finite element modeling using a multi-physics solver package was performed to characterize the flow field through the impactor, the wake and far field regions. To simplify the model, the computational domain was represented by a longitudinal cut of the flow domain centered on one of the slits on the impactor. A two-dimensional model was used with symmetric flow conditions on the upper and lower boundaries of the flow domain to reflect the symmetry of the flow approaching each of the eight orifice slits. For modeling the fluid flow, a turbulent κ-ω model (turbulent model based on turbulent kinetic energy, κ and dissipation of turbulent kinetic energy, ω) was used with a uniform velocity inlet at the upstream boundary (left) and a pressure outlet condition at the downstream boundary. The computational grid was composed of approximately of 80,000 elements.

The results of the simulation are presented in Figs. 3 and 4. In the close-up plot of the velocity contour field, shown in Fig. 3, a well-defined jet is seen impinging on the impactor surface. As the flow progresses around the impactor plate, the symmetric boundaries impose additional flow constraints preventing additional spreading and bounding the flow to a narrow shear stream, on the top and bottom boundaries, in the longitudinal direction. Figures 4a and 4b show the velocity vector (unit arrow length) plot and streamline plot respectively of the flow through the impactor stage and some distance downstream. In addition to the high turning angles at the impactor surface, strong velocity gradients of flow curvature are seen on the upstream side of the orifice plate near the orifice opening, as well as on the back side of both impaction bands. Although these gradients are not as strong as those encountered on the upstream impaction surface, they are potentially another source of particle losses to these surfaces. Since the

arrows on the vector are unit length, they should only be used to interpret flow direction and not the magnitude of the flow. The high velocity shear flow near the upper and lower boundaries induces a large recirculation region directly behind the impactor band, which is markedly shown in the streamline plot of Fig. 4b. Although the strength (velocities) of the recirculation is low, the size of the recirculation region is rather extensive when compared to the jet geometry and therefore can also be a source of particle losses since particle are hindered from advecting further downstream.

The simulations can be used to find values of the jet velocity based on measured upstream flow conditions. The jet velocities are then used in the equations of Section III to calculate the particle cut sizes d_{50}. Applying the measured inlet velocities the following jet velocities and cut sizes were found: 4, 5.37, and 6.89 m/s and 4.6, 4.2 and 3.7 μm respectively.

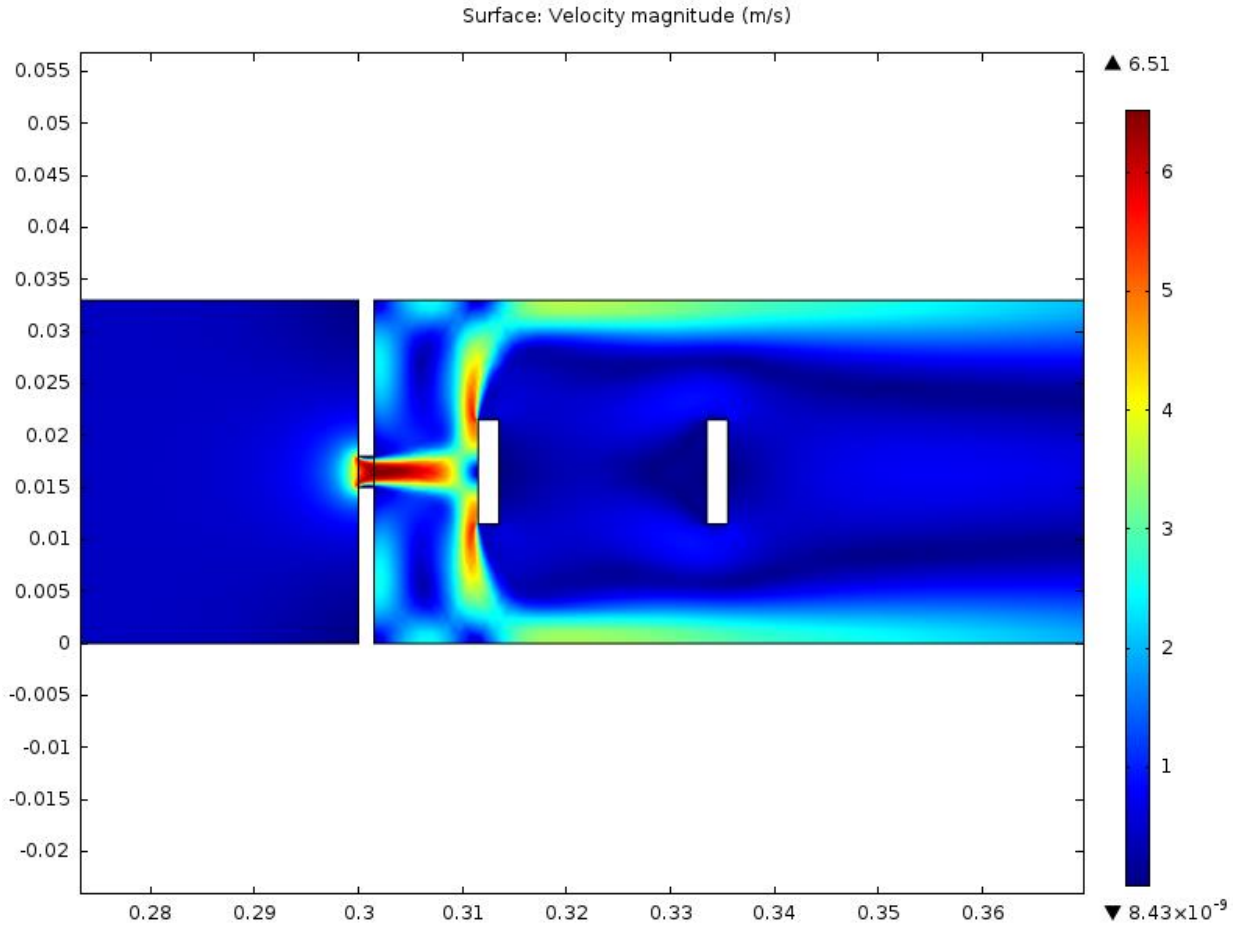

Figure 3: Velocity contour plot of impactor flow.

(a)

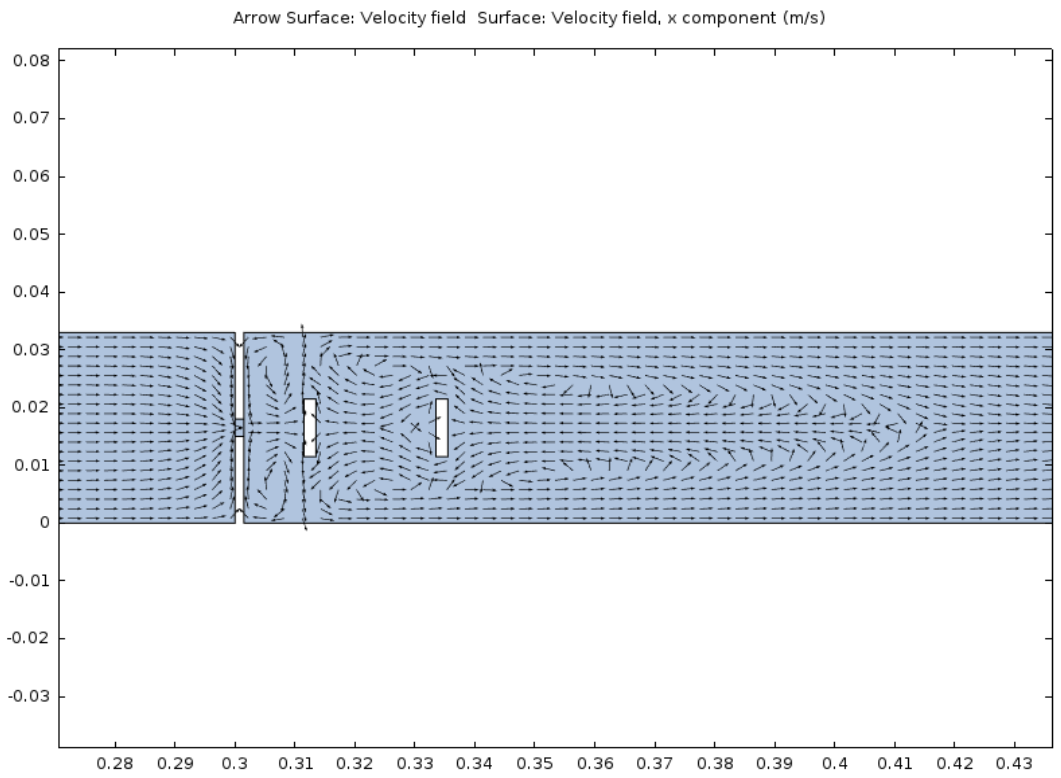

(b)

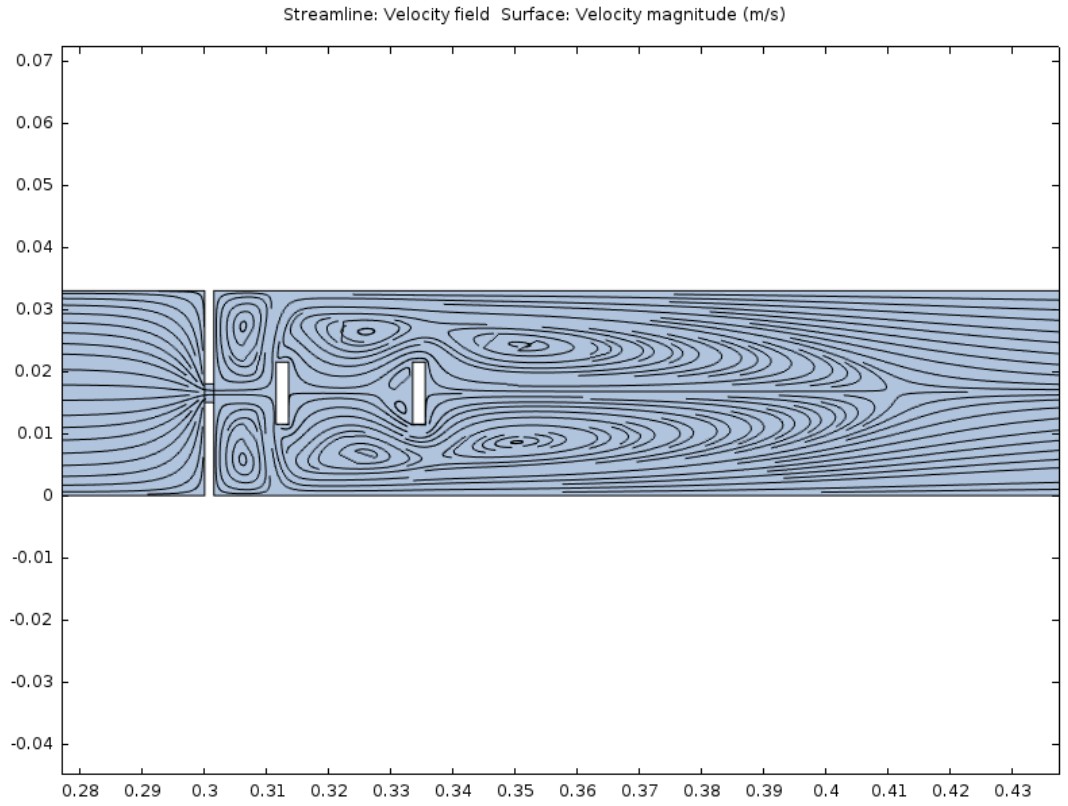

Figure 4: (a) velocity vector plot (unit arrow size), (b) Streamline plot of impactor flow.

V. Experimental Setup

A flow loop schematic of the experimental setup is given in Fig. 5. As will be discussed, the current experimental setup has three main improvements over previous setups: (1) a longer entrance duct; (2) a pneumatic particle generator which produces high particle counts; and (3) a cascade impactor for concentration measurements.

The entrance duct (first duct section) is 30 cm x 30 cm x 91 cm long. The purpose of the entrance duct is to facilitate the introduction of the challenge aerosol. The inlet HEPA filter removes any secondary particle sources and provides a clean air environment in which to introduce the challenge aerosol. The next section is the impactor stage section (the endless belt is represented inside this stage), and the last duct section is used for sampling downstream particle concentrations. The main HEPA vacuum cleaner drives the flow through the ducts interfacing at the outlet conic duct section, and provides up to 0.052 m^3/s (110 CFM) of standard air flow. Measurements of face velocities developed in the entrance duct are nominally in the range of 0.3 to 0.48 m/s. Particles are introduced into the flow just downstream of the inlet HEPA filter through a pneumatic particle dispenser. The particles are injected through a stainless steel tube and directed against the incoming flow, as prescribed in ASHRAE standard 52.7[5], to ensure good mixing and lateral spreading of the particle flow as it heads downstream. The length of the entrance duct was important in providing enough distance for the particles to spread from the source injection. Commercially available powders of mono-size (within 10% tolerance) spherical silica particles where used to generate the challenge aerosols. Additionally, JSC-1af lunar simulant powder (see Ref. 6 for properties) was also used to provide an aerosol with a broad size distribution and an extended upper size range. Some dilution of the particle flow from the generator was needed to maintain moderate levels of particle concentration that would not overwhelm the measuring instrument.

Particle concentrations are measured upstream and downstream of the impactor stage using a cascade impactor. The instruments measures real-time mass concentration over ten channel stages from 0.1 to 10 µm (specifically 0.1, 0.2, 0.3, 0.45, 0.7, 1.4, 2.5, 4, 7, and 10 µm) using an active quartz crystal microbalance (QCM) to provide direct mass measurements in each stage. Each stage of the impactor has a different diameter orifice which controls the cut-size of impacted particles for that particular stage. Only one sample can be taken at a time, and therefore during testing the sampling lines are alternated at the inlet to the instrument between the upstream and downstream probes. Fig. 5 shows the upstream probe connected in this instance. The instrument uses a controller to actuate an inlet valve and to power and measure the QCM during sampling. The controller is interfaced to a laptop to log and store the data.

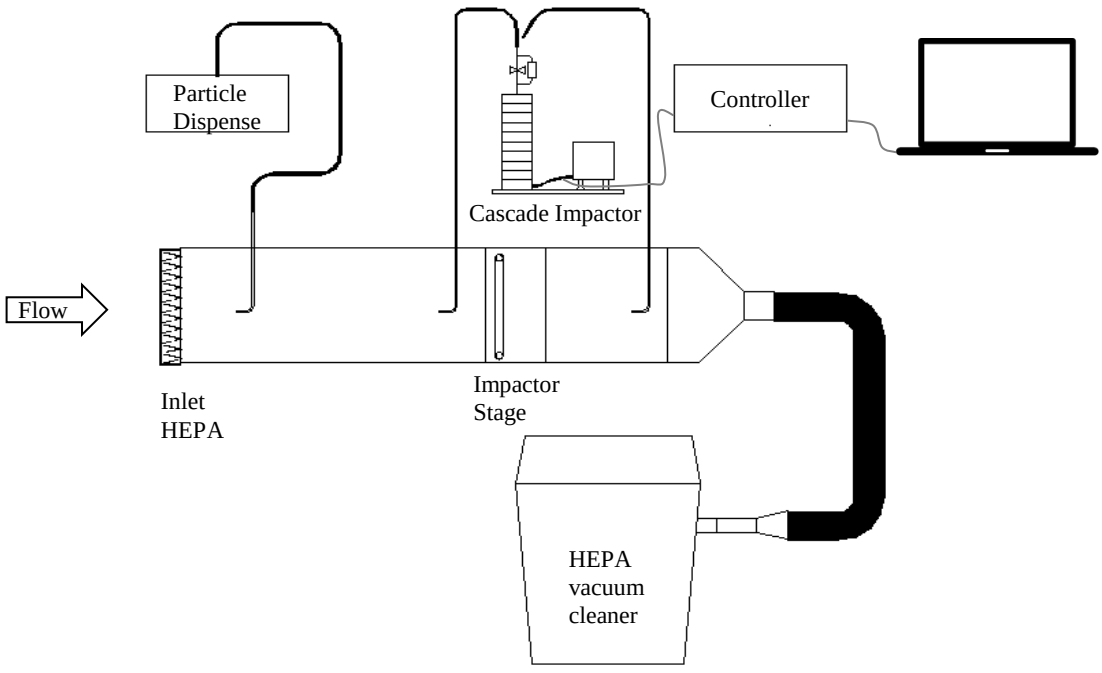

Figure 5: Experimental Setup.

VI. Results

In order to measure the collection efficiency in a controlled manner the upstream particle generation needed to be fairly consistent. Figure 6 shows the particle size distribution measured over consecutive runs for the two different sizes of the challenge silica particles and the JSC-1af lunar simulant. The plots of the silica particles, Figs. 6a and 6b, show that the peak concentration values are centered about the nominal size of the silica particle and extend to within one measured particle size of the instrument. For instance, the peaks for the 0.25 µm silica particle test runs are spread over the 0.2 µm to 0.45 µm particle sizes. These peak concentration values were the ones selected for further data analysis of collection efficiency because of their higher statistical significance. It should be noted that the width of the 3.0 µm silica particle distribution may be over-represented in the 1 µm to 4 µm size range because of the large gap is consecutive channel sizes of the instrument in this range – i.e. there may be a big drop-off between 2.5 µm and 4 µm which is not measured. As expected, the distribution of the lunar simulant appears to be broad and well distributed because of the polydisperse nature of the simulant. In general, the concentrations were sufficiently large to provide a good level of signal-to-noise ratio in the upstream measurements. However, concentration levels above the 4 µm particle size were very low and unusable even in the lunar simulant case. The downstream concentration measurements, although typically lower, were also resolved with an adequate ratio of signal-to-noise levels. While the particles are mono-dispersed at the source, the broader than single-peak distributions indicate that there was some degree of agglomeration that the pneumatic particle generator could not break up. Also any small amount of smaller particles, smaller than the nominal size of the particles, were assumed to be a remnant from previous fillings of the particle generator and/or some attrition of the base particles. The plots show that the concentrations are more or less consistent from one instance to the next for each nominal particle size used. There was more scatter at the smaller particle size, indicating more uncertainty in the measurements at this size. The difference in concentration levels among the two silica sizes and the lunar simulant could be explained by considering the aerodynamics of the differently sized and shaped particles and any differences in internal conveying of the powders to the pneumatic air source inside the particle generator. To reduce some of the uncertainty, measurements were alternated between the upstream and downstream probes several times, and each pair of consecutive measurements were used separately to calculate efficiencies.

To calculate the collection efficiency of the impactor stage, the ratio of the measured particle concentrations upstream and downstream were used in the following relation:

$$\varepsilon = 1 - \frac{N_{downstream}}{N_{upstream}} \tag{4}$$

Where N is the concentration measurement.

Figure 7 shows the collection efficiency obtained for three different inlet flow velocities tested. Each plot contains measurements obtained with both the silica and lunar simulant particles. Only measurements centered on the nominal silica particle size, as discussed previously, and from 1.4 µm to 4 µm for the lunar simulant were used in the efficiency plots. Classical cut curves for the corresponding inlet velocity are superimposed on each of the graphs. Except at the largest measured particle size, 4 µm, the trend seems to show a departure from those of a classical impactor. In fact, significantly higher collection efficiencies were obtained for particle sizes much smaller than the impactor cut size (calculated from the equations in Section III). Factors that may explain this are particle losses on the front face of the orifice plate and from particles entrained in the recirculation region, or zones, behind the impactor bands, as seen in the modeling results. The recirculation zones may act as a buffer region where the residence time of the particles is significantly increased. The latter effect may promote agglomeration of the particles which then eventually settle out further downstream. Natural settling of the particles in the flow over the approximately 50 cm distance between the upstream and downstream probes did not likely result in any significant particle loss. Calculations of particle settling, of the largest diameter particle, were found to be only in the range of 2 to 3 mm over the distance between the probes. Also measruments of upstream and downstream concentration were conducted in the test rig, in the absence of the impactor plate and bands, which indicated little to no loss of concentration between the probe locations. Another aspect to consider is that impactor calibration curves are typically obtained by comparing the incoming particle concentration against the particle mass collected and measured on the impactor stages. In the present experimental setup this was not possible, therefore an "apples to apples" comparison with classical impactor curves is not exactly appropriate here. Lastly, a comparison of the present collection efficiency data, for particles in the size range of 1 µm to 4 µm and for the highest inlet velocity

case, were found to be within 14% of previous low-g data, thereby providing some confirmation of the previous flight data and test methods.

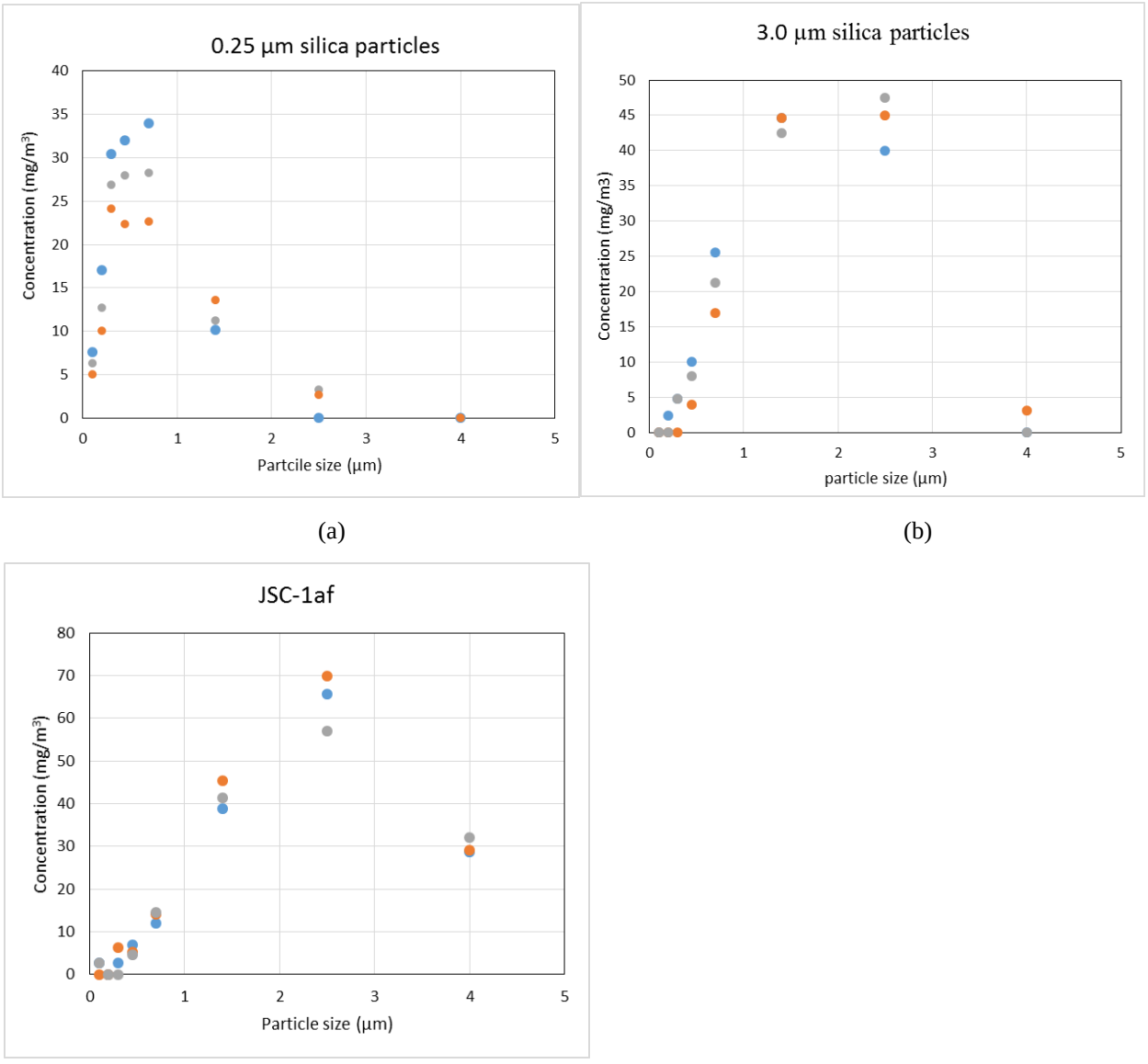

Figure 6: Upstream concentration measurements for (a) 0.25 µm silica particles, (b) 3.0 µm silica particles, and (c) JSC-1af lunar simulant.

Figure 7: Collection efficiency curves for different inlet velocities: (a) 0.3 m/s, (b) 0.36 m/s, (c) 0.46 m/s. The corresponding theoretical impactor cut size curve (dotted curve) is superimposed on each graph.

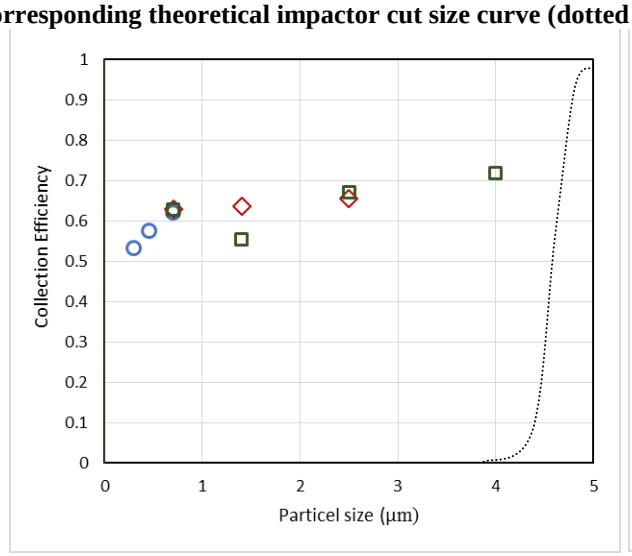

(a)

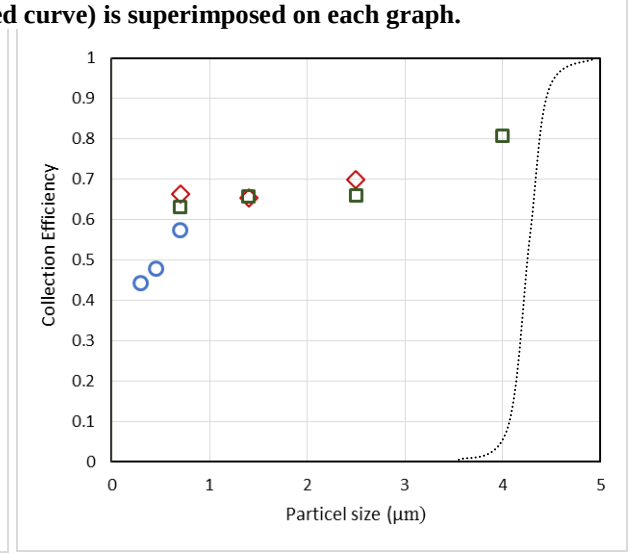

(b)

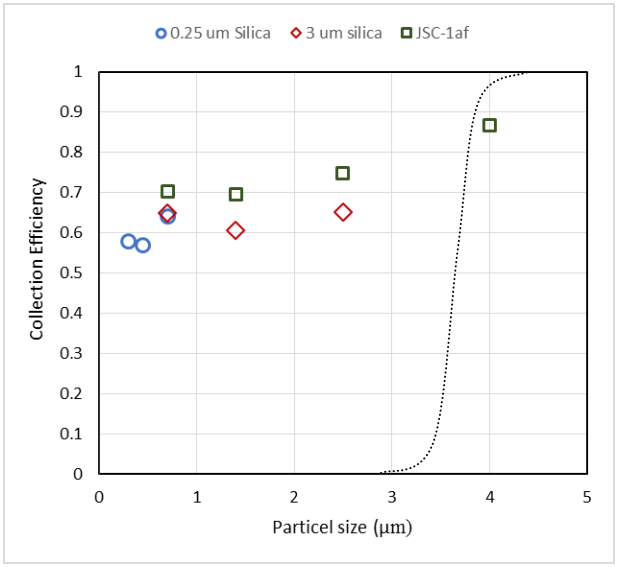

(c)

Figure 7: Collection efficiency for different inlet velocities: (a) 0.3 m/s, (b) 0.36 m/s, (c) 0.46 m/s. The corresponding theoretical impactor cut size curve (dotted curve) are superimposed on each graph.

VII. Conclusion

The performance of a new type of regenerable filter system using impaction principles has been tested. Previous results of testing in parabolic flights revealed that further studies were needed for confirmation and demonstration under more controlled conditions than the short periods of microgravity would allow. A new setup using a long entrance duct, a pneumatic particle generator, and a virtual cascade impactor instrument provided better quality performance data on the filter. The performance trends indicated that the particle collection efficiency of the impactor filter approached that of the classical impactor, of an equivilant design cut size, at the largest particle size measured, yet resulted in significantly better collection efficiency for particle sizes much smaller than the cut size. These results are consistent with previoiusly obtained flight test data under low-g test conditions. Factors that may explain the greater efficiency results are particle losses on the front face of the orifice plate and from particles

entrained in the recirculation zones behind the impactor bands, revealed by the modeling. The recirculation zones may have acted as a buffer region where the residence time of the particles was significantly increased. Future modeling of particle transport in the flow through the impactor stage and in its wake can help resolve the disparity.

References

[1]Meyer, M "ISS Ambient Air Quality: Updated Inventory of Known Aerosol Sources," 44th International Conference on Environmental Systems ICES 17 July 2014, Tucson, Arizona.

[2]Green, R.D., Vijayakumar, R. and Agui, J.H. "Development of test protocols for International Space Station particulate filters," 44th International Conference on Environmental Systems ICES 17 July 2014, Tucson, Arizona.

[3]Agui, J.H and Vijayakumar, R. "Development of an Indexing Media Filtration System for Long Duration Space Missions," 44th International Conference on Environmental Systems ICES 17 July 14-18, 2013, Vail, CO.

[4]Hering, S. V. 1995. Impactors, cyclones, and other inertial and gravitational collectors. In *Air Sampling Instruments*, B. S. Cohen and S. V. Hering (Eds), Cincinnati, OH.

[5]American Society of Heating, Refrigeration and Air-Conditioning Engineers (2007) "Method of Testing General Ventilation Air-Cleaning Devices for Removal Efficiency by Particle Size," ASHRAE 52.2-2007

[6]URLlink:
http://isru.msfc.nasa.gov/lib/workshops/2009/03_JSC1A_Lunar_RegSimulant_Update_BGustafson.pdf.